Simulation of Shock-Tube Flows with Detailed Finite-Rate Chemistry by the CESE Method

David L. Bilyeu*, S.-T. John Yu.†
The Ohio State University, Columbus, OH 43210

and

Douglas Davis‡
Air Force Research Laboratory
Wright Patterson Air Force Base, Dayton, OH 45433

The present paper reports the development of a high-fidelity numerical tool to model shock tube flows with detailed finite-rate chemistry models. The goal is to aid the shock-tube experiments for studying combustion in scramjet engines. The space-time Conservative Element and Solution Element (CESE) method is employed to solve the Euler equations for chemically reacting flows. The source terms of the species equations are integrated by using an efficient ODE integrator provided by Cantera with sub-time steps. The effect of these source terms are treated as an integral part of the space-time flux conservation in the setting of the CESE method. In this paper, two chemistry models are employed: (i) the GRI Mech 3.0 model for CH_4/air reactions with 54 species and 325 reaction steps, and (ii) Wang's 1999 C_2H_4/O_2 mechanism with 76 species and 529 reactions. Systematic code validation and verification are performed to obtain required space-time resolution for accurate prediction of ignition delay time for both fuels under various thermodynamic conditions. The present shock-tube tool can be used to assist further development of chemistry models and to aid shock-tube experimental data analysis for combustion of heavy hydrocarbon fuels to be used in scramjet engines.

Nomenclature

$\mathbf{A}$	=	jacobian matrix
$\tilde{\mathbf{A}}$	=	jacobian matrix for non-conservative equations
A_{fj}	=	forward Arrhenius rate coefficient for reaction j
C_p	=	specific heat at constant pressure
C_v	=	specific heat at constant volume
E	=	specific total energy
E_{fj}	=	forward Arrhenius activation energy for reaction j
e	=	specific internal energy
$\boldsymbol{F}$	=	flux terms
f_m	=	m^{th} flux variable
K_{bj}	=	backward reaction rate for reaction j
K_{cj}	=	equilibrium constant for reaction j
K_{fj}	=	forward reaction rate for reaction j
k	=	sub-time step number
M_i	=	molecular weight
N_r	=	number of reactions
N_s	=	number of species

* Graduate Research Associate, Mechanical Engineering Dept., Email: bilyeu.4@osu.edu; AIAA Student Member.
† Associate Professor, Mechanical Engineering Dept., Email: yu.274@osu.edu; AIAA Member.
‡ Aerospace Engineer, AFRL/RZAS, Email: Douglas.Davis@wpafb.af.mil

n_{fj} = forward temperature exponent in Arrhenius equation
p = pressure
p_o = reference pressure
p_e = partial derivative of pressure with respect to internal energy
p_ρ = partial derivative of pressure with respect to total density
$p_{\rho i}$ = partial derivative of pressure with respect to density of species i
R_c = universal gas constant (energy units in calories)
R_i = specific gas constant
R_o = universal gas constant (energy in joules)
$\mathbf{S}, \tilde{\mathbf{S}}$ = source terms
t = time
T = temperature
$\mathbf{U}$ = conservative variables
$\tilde{\mathbf{U}}$ = non-conservative variables
u_m = m^{th} flow variable
v = velocity
x = spatial distance
Y_i = mass fraction of species i
Δx = grid size
ΔG_i = change in Gibbs free energy
Δt = physical time step
Δt_c = chemical time step
λ = eigenvalues
ν'_{ji} = stoichiometric coefficients of the products for reaction j and species i
ν''_{ji} = stoichiometric coefficients of the reactants for reaction j and species i
$\dot{\omega}_i$ = source terms for species i
Ω = space time domain
ρ = density

I. Introduction

DESIGNING dual-mode scramjets to operate at lower Mach number (≈ 5) would be benefitted by a better understanding of low-temperature combustion kinetics of hydrocarbon fuels. To obtain kinetics data one could use a shock tube, in which a mixture of fuel, oxidizer, and bath gases is instantly raised to higher temperatures by shock reflection, leading to auto-ignition of the gas mixture. Shock-tube data has been analyzed based on the assumption of constant-volume processes. Using a thermodynamics/kinetics tool, e.g., CHEMKIN, for processing the shock-tube data has been the common practice. However, for combustion inside a dual-mode scramjet engine, many conventional assumptions for analyzing shock-tube flows become inaccurate because of the anticipated long ignition delay of the fuel/air mixtures. To this end, one has to incorporate a time-accurate flow solver with the thermodynamics/kinetics calculations. The primary goal of the present research is to develop a high-fidelity numerical tool to investigate interactions between flow, finite-rate chemistry, and thermodynamics in shock-tube flows for studying low-temperature combustion in scramjet combustor. As a part of code verification and validation, this shock-tube tool must be able to accurately reproduce the measured ignition delays of standard hydrocarbon fuels under various operational conditions. Such accuracy assessment of course must be anchored by shock-tube experimental data, for which the conventional data reduction process has been relying on zero-dimensional calculations and thus must be improved. The proscribed initial conditions are generally found by using the measured shock speed and the initial conditions inside the test section of the shock tube experiments.[1,2] Ideal fluid conditions are usually assumed, including well-mixed condition with uniform pressure and temperature, which are may not be true.

In addition to processing the shock-tube data, zero-dimensional calculations have been routinely used by chemists to assess the accuracy of simplified finite-rate mechanisms, developed for CFD modeling for chemically reacting flows in two and three spatial dimensions. The use of a full mechanism, which usually involved dozens of species and hundreds of reactions steps, for CFD modeling for combustion of even the simplest hydrocarbon fuels is still beyond the current computer capacities. Instead, reduced mechanisms have been commonly used in modeling chemically reacting flows. In general, for two- and three-dimensional CFD simulations, one could afford to

incorporate 10 to 20 species equations to accommodate the limited computer resources and the required fast turnaround time. The accuracy of such simplified mechanisms has only been validated by zero-dimensional calculations for certain ranges of conditions. When coupled with a two- or three-dimensional CFD code, the accuracy of these mechanisms as a function of the spatial and temporal resolution in the CFD calculations has not been systematically examined. In particular, spatial resolution is a major concern. While it is the general consensus that further development of novel scramjet engine concepts will heavily reply on CFD prediction, lack of code verification and validation for CFD simulation using reduced finite-rate chemistry models is one technical obstacle yet to be addressed. In this paper, we will report the required spatial and temporal resolution to ensure numerical accuracy in calculating certain hydrocarbon fuels in shock tubes. A validated shock-tube tool could be used to systematically test the accuracy of the proposed skeleton mechanisms by comparing the calculated ignition delays with the known data or with the predicted ignition delay times by using the full chemistry models. Such a modeling tool can also serve as a testing bed to ascertain the required spatial and temporal resolution before the full three-dimensional CFD simulation of complex chemically reacting flows.

A shock tube is an ideal tool for studying ignition delays of fuel/air mixtures. A shock tube can produce rapid increases in both pressure and temperature with minimal changes to the initial species composition. A shock tube is a long tube with either a circular or rectangular cross section with a barrier dividing two separate gasses. One gas known as the driver gas has its pressure elevated and is normally composed of a non-reacting gas such as argon. On the other side of the barrier, the driven gas has lower pressure and is composed of a fuel/oxidizer mixture, often diluted by an inert gas, e.g., Ar or N_2. The fuel/oxidizer mixture is normally diluted by about 80-95%.[3] At the beginning of the experiment, the barrier is removed either though a material failure or a valve. Due to the pressure difference, the rupture of the barrier allows a shock wave to move towards the driven side leading to increased temperature and pressure behind the shock front. The shock wave will reflect off the closed end of the tube, which will drastically increase the temperature and pressure of the test gas at the closed end. The removal of the barrier will also create an expansion wave that moves in the opposite direction with respect to the shock through the driver gas. The rarefaction wave decreases the temperature and pressure behind it. Similarly to the shock wave, the rarefaction wave will reflect from the far end and move back towards the driven gas.

In general, the test time for a typical shock tube experiment is limited to be less than a few milliseconds. This test time period is adequate for studying combustion of simple fuels, e.g., hydrogen, because of its short ignition delay time. However, when applying standard shock tubes to study complex hydrocarbon fuels with much longer ignition delay times, the measurements will be complicated by complex traveling waves, including interaction between the contact discontinuity and the reflected shock, the cooling-down effect when the reflected rarefaction wave reaches the testing zone, etc. The shock-tube experiments, which do not pose a problem for testing simple fuels such as hydrogen, can have major problems when used to test heavy hydrocarbon fuels at low temperatures.

Although hydrogen was used in scramjets for the NASP programs[4], our main concern in the present work is to study combustion of hydrocarbons in a dual-mode scramjet engine. In particular, the current development of X-51A scramjet[5]by the Air Force Research Lab at Wright Patterson is of interest. The X-51A is a liquid hydrocarbon fueled scramjet engine. To date, extensive ground tests have been performed. The first flight test is scheduled to be performed in August 2009. The fuel used in X-51A is also used to remove excessive heat of the scramjet engine. When the fuel heats up, it will undergo pyrolysis and thermal cracking. During this process, the heavier hydrocarbons break down to lighter molecules. A successful thermal cracking process would produce unsaturated hydrocarbons such as ethylene, but not other saturated hydrocarbons, e.g., methane, ethane, and/or coke (solid carbon)[6]. Another possible outcome of using the fuel as a coolant is that the induction delay time will decrease. This is due to the raised temperature of fuel as it enters the combustor, and a higher concentration of lighter hydrocarbons which have a shorter induction time. Studies on induction time has been performed and found that there is a slight decrease in the induction time with additional light hydrocarbons[7,8].

One problem when studying hydrocarbon fuels is that the induction time, or time it takes for the fuel to start to combust, is much longer than typical flow residence time for most of shock tubes. There are two main limiting time scales: (i) *The dwell time*: the time period that starts when the shock wave reflects off of the end wall and ends when reflected expansion wave starts to cool down the reacting gases[9]. (ii) *The interaction time*: the time period between the shock reflection and the interaction between the reflected shock and the contact discontinuity wave. The reflected shock from the closed end of the shock tube would collide with the incoming contact discontinuity, which is moving towards the closed end. There are three possible outcomes to this interaction: (i) a shock wave will propagate back into the test gas increasing the temperature and pressure, (ii) an expansion wave will propagate back into the test gas decreasing the temperature and pressure or (iii) the reflected shock wave will pass through the contact without reflecting back[10].

The third case allows for longer test time which is required when the induction time becomes longer than the maximum test time allowed by a particular shock-tube experiment, e.g., in low-temperature combustion of heavy hydrocarbons. This can be achieved by matching the speed of sound and the specific heat of the reflected gas with that of the gas behind the contact discontinuity[10]. This has normally been done by using a mixture of He/Ar or He/N_2 but there has been recent studies done using other heavy gasses such as refrigerants, carbon dioxide and propane[11]. After the interaction, the contact discontinuity becomes stationary. These complex wave interactions could greatly complicate the data analysis of shock-tube experiments. This flow phenomenon is one example why applying shock-tube experiments to study low-temperature, low-pressure combustion of heavy hydrocarbons has been difficult.

As an example of the high-fidelity simulation by using our newly developed code, Figures 1 and 2 show the comparison of shock-tube flows between using untailored gases and tailored gases. Figure 1 shows the space-time temperature contours of an untailored shock tube experiment where the reflected shock wave will reflect off of the contact discontinuity and further increase the temperature of the test gas. The initial conditions of the shock-tube experiment are that of Case 1 in Table 1. Figure 2 shows the space-time plot of temperature of tailored shock tube experiment, where the reflected shock wave does not reflect off of the contact discontinuity. The initial conditions of this simulation are shown in Case 2 in Table 1 but the driver pressure is reduced to 0.2647 (atm) and the driver gasses are 91.21% He and 8.79% Ar. These two plots show the advantages of our new tools over the conventional zero-dimensional calculation for shock-tube experiments. Moreover, to study kinetics of heavy hydrocarbons at low temperatures and low pressures, the result here clearly show the importance of gas tailoring for controlling the viable testing time in the shock tube experiments.

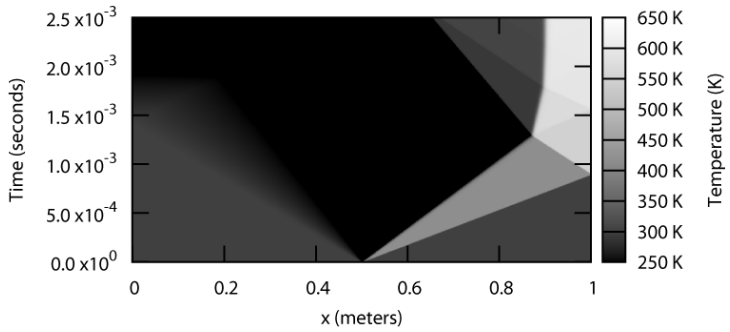

Figure 1: Space-time plot of temperature for wave interactions in an un-tailored shock tube.

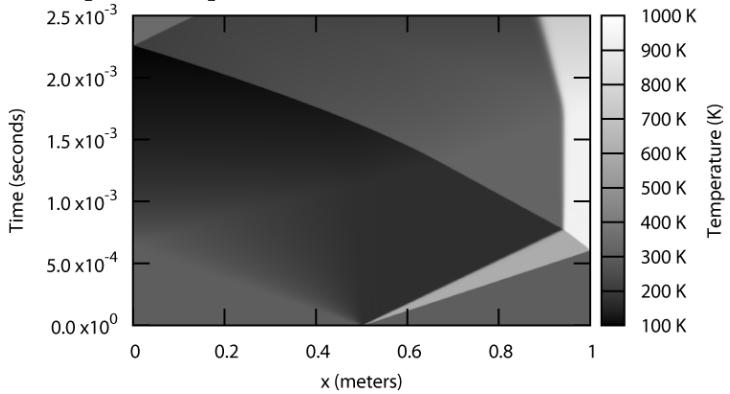

Figure 2: Space-time plot of temperature for wave interactions in a tailored shock tube.

An accurate CFD tool for shock tube could greatly enhance the analyses of the shock tube data for studying combustion of heavy hydrocarbons. Aided by a CFD tool, one can carefully design the experiments with suitable gas tailoring such that complex wave interactions could be minimized or totally avoided. Accurate estimation for time histories of pressure and temperature in the test zone of the shock tube could be obtained before the experiment such that a window of operation for viable scramjet engine conditions could be identified.

The optimum goal of this research is to predict the ignition delay times of complex hydrocarbons of aviation fuels such as JP-7. JP-7 is a blended fuel. Its composition is a combination of several different compounds which can be estimated as $nC_{13}H_{26}$. When cracked, the main compounds are methane, ethylene, ethane, propylene and propane[6]. As a first step to accurately model JP-7 combustion, we report the modeling of the constituent fuels. This

involves determining the required time and space scales to produce accurate inductions delay times for methane ethylene, propane, etc. To demonstrate the capabilities of the newly developed shock-tube tool, we will report the simulations ignition of CH_4/air and C_2H_4/O_2/Ar mixtures in the present paper. Comprehensive finite-rate chemistry models by Wang for C_2H_4 combustion[12] and GRI Mech 3.0 for CH_4 combustion[13] are employed in the present paper. The result is a steppingstone for further detailed simulations of other heavier fuels.

To recap, the newly developed numerical tool can be used to (i) calculate the ignition delay times for various fuel/air mixtures at a wide range of initial conditions, (ii) to serve as a test bed to assess the accuracy of simplified chemistry models for two- and three-dimensional CFD calculations, and (iii) to facilitate the use of the shock tube experiments to study chemical reactions of heavy hydrocarbons to be used in a dual-mode scramjet engine. The rest of this paper is organized as follows. Section 2 illustrates the model equations. Section 3 shows the CESE method. Section 4 reports the results. We then provide the concluding remarks and cited references.

II. Model Equations

A. Reacting Flow Equations

The governing equations are one-dimensional multi-species Euler equations, including conservation of mass, momentum, and energy, and a set of N_s-1 species equations. The gas mixture includes N_s species. The density of the unsolved species can be calculated by mass conservation. The model equations are cast into the following vector form:

$$\frac{\partial \mathbf{U}}{\partial t} + \frac{\partial \mathbf{F}(\mathbf{U})}{\partial x} = \mathbf{S}(\mathbf{U}), \tag{1}$$

where

$$\begin{aligned} \mathbf{U} &= \left(u_1, u_2, ..., u_{N_S+2}\right) = \left(\rho, \rho v, \rho E, \rho_1, \rho_2, ..., \rho_{N_S-1}\right)^T, \\ \mathbf{F} &= \left(f_1, f_2, ..., f_{N_S+2}\right) = \left(\rho v, \rho v^2 + p, (\rho E + p)v, \rho_1 v, \rho_2 v, ..., \rho_{N_S-1} v\right)^T, \\ \mathbf{S} &= \left(s_1, s_2, ..., s_{N_S+2}\right) = \left(0, 0, 0, \dot{\omega}_1, \dot{\omega}_2, ..., \dot{\omega}_{N_S-1}\right)^T, \end{aligned} \tag{2}$$

where ρ, v, E, ρ_i and ω_i are the density, velocity, total specific energy, density of the i^{th} species, and species production rate of the i^{th} species, respectively. Aided by the chain rule, Eq. (1) becomes

$$\left(\frac{\partial \mathbf{U}}{\partial t}\right) + \mathbf{A}\left(\frac{\partial \mathbf{U}}{\partial x}\right) = \mathbf{S}(\mathbf{U}) \tag{3}$$

where the Jacobian matrix A is defined as

$$\mathbf{A} = \frac{\partial \mathbf{F}}{\partial \mathbf{U}} \tag{4}$$

The density of the gas mixture is equal to the sum of all of the species density, i.e. $\rho = \sum_{i=1}^{N_s} \rho_i$. The specific total energy is defined as

$$E = e + \frac{v^2}{2}, \tag{5}$$

where e is the specific internal energy and is calculated by

$$e = \sum_{i=1}^{N_S} Y_i e_i \tag{6}$$

with Y_i as the mass fraction of species i

$$Y_i = \frac{\rho_i}{\rho}. \tag{7}$$

The specific internal energy for a species, e_i, is calculated by

$$e_i = h_i - R_i T \tag{8}$$

where h_i is the enthalpy of species i and is a function of temperature only because of the assumption of ideal gases. R_i is the gas constant of species i. Based on the ideal-gas assumption, the enthalpy and specific heat of a particular species can be calculated from a set of polynomials of temperature as that in the standard NASA CEA program.

The Euler equations are solved using the Space-Time Conservation Element Solution Element (CESE) method. To derive the Jacobian matrix **A**, we convert Eq. (1) into its non-conservative form

$$\frac{\partial \tilde{\mathbf{U}}}{\partial t} + \tilde{\mathbf{A}} \frac{\partial \tilde{\mathbf{U}}}{\partial x} = \tilde{\mathbf{S}} \tag{9}$$

where

$$\begin{aligned} \tilde{\mathbf{U}} &= \left(\tilde{u}_1, \tilde{u}_2, ..., \tilde{u}_{N_s+2}\right)^T = \left(\rho, v, e, \rho_1, \rho_2, ..., \rho_{N_s-1}\right)^T \\ \tilde{\mathbf{S}} &= \left(\tilde{s}_1, \tilde{s}_2, ..., \tilde{s}_{N_s+2}\right)^T = \left(0, 0, 0, \dot{\tilde{\omega}}_1, \dot{\tilde{\omega}}_2, ..., \dot{\tilde{\omega}}_{N_s-1}\right)^T \end{aligned} \tag{10}$$

Straightforward derivation shows that

$$\tilde{\mathbf{A}} = \begin{bmatrix} v & \rho & 0 & 0 & 0 & \cdots & 0 \\ \frac{p_\rho}{\rho} & v & \frac{p_e}{\rho} & \frac{p_{\rho_1}}{\rho} & \frac{p_{\rho_2}}{\rho} & \cdots & \frac{p_{\rho_{N-1}}}{\rho} \\ 0 & \frac{p}{\rho} & v & 0 & 0 & \cdots & 0 \\ 0 & \rho_1 & 0 & v & 0 & \cdots & 0 \\ 0 & \rho_2 & 0 & 0 & v & \cdots & 0 \\ \vdots & \vdots & \vdots & \vdots & \vdots & \ddots & \\ 0 & \rho_{N-1} & 0 & 0 & 0 & & v \end{bmatrix} \tag{11}$$

Where p_ρ, p_e and $p_{\rho i}$ are equal to

$$\begin{aligned} p_\rho &= \left(\frac{\partial p}{\partial \rho}\right)_{e,\rho_i} = \frac{R_o T}{M_{N_s}} + \frac{R}{C_v} \sum_{i=1}^{N_s-1} \frac{\rho_i}{\rho} \left(e_i - e_{N_s}\right), \; i = 1, \cdots, N_s - 1 \\ p_e &= \left(\frac{\partial p}{\partial e}\right)_{\rho,\rho_i} = \frac{\rho R}{C_v}, \; i = 1, \cdots, N_s - 1 \\ p_{\rho_i} &= \left(\frac{\partial p}{\partial \rho_i}\right)_{\rho,e,\rho_l} = -\frac{R}{C_v}\left(e_i - e_{N_s}\right) + R_o T \left(\frac{1}{M_i} - \frac{1}{M_{N_s}}\right), \quad l = 1, \cdots, N_s - 1, \; j \neq i \end{aligned} \tag{12}$$

A detailed derivation of the above equations can be found in Bilyeu[14]. The non-conservative form of the governing equation can be transformed back into the conservative form by pre-multiplying Eq. (9) by ($\partial \mathbf{U} / \partial \tilde{\mathbf{U}}$) yielding,

$$\left(\frac{\partial \mathbf{U}}{\partial \tilde{\mathbf{U}}}\right)\left(\frac{\partial \tilde{\mathbf{U}}}{\partial t}\right) + \left(\frac{\partial \mathbf{U}}{\partial \tilde{\mathbf{U}}}\right)\tilde{\mathbf{A}}\left(\frac{\partial \tilde{\mathbf{U}}}{\partial \mathbf{U}}\right)\left(\frac{\partial \mathbf{U}}{\partial \tilde{\mathbf{U}}}\right)\left(\frac{\partial \tilde{\mathbf{U}}}{\partial x}\right) = \left(\frac{\partial \mathbf{U}}{\partial \tilde{\mathbf{U}}}\right)\tilde{\mathbf{S}} \tag{13}$$

Note that an identity matrix $\mathbf{I} = \left(\frac{\partial \tilde{\mathbf{U}}}{\partial \mathbf{U}}\right)\left(\frac{\partial \mathbf{U}}{\partial \tilde{\mathbf{U}}}\right)$ has been inserted into the convection term of the above equation. By comparing Eq. (3) and (13), we have

$$\mathbf{A} = \left(\frac{\partial \mathbf{U}}{\partial \tilde{\mathbf{U}}}\right)\tilde{\mathbf{A}}\left(\frac{\partial \tilde{\mathbf{U}}}{\partial \mathbf{U}}\right) \tag{14}$$

where

$$\frac{\partial \mathbf{U}}{\partial \tilde{\mathbf{U}}} = \begin{bmatrix} 1 & 0 & 0 & 0 & 0 & \cdots & 0 \\ v & \rho & 0 & 0 & 0 & \cdots & 0 \\ E & \rho v & \rho & 0 & 0 & \cdots & 0 \\ 0 & 0 & 0 & 1 & 0 & \cdots & 0 \\ 0 & 0 & 0 & 0 & 1 & \cdots & 0 \\ \vdots & \vdots & \vdots & \vdots & \vdots & \ddots & \\ 0 & 0 & 0 & 0 & 0 & & 1 \end{bmatrix} \tag{15}$$

and

$$\frac{\partial \tilde{\mathbf{U}}}{\partial \mathbf{U}} = \begin{bmatrix} 1 & 0 & 0 & 0 & 0 & \cdots & 0 \\ -\frac{v}{\rho} & \frac{1}{\rho} & 0 & 0 & 0 & \cdots & 0 \\ \frac{v^2 - E}{\rho} & -\frac{v}{\rho} & \frac{1}{\rho} & 0 & 0 & \cdots & 0 \\ 0 & 0 & 0 & 1 & 0 & \cdots & 0 \\ 0 & 0 & 0 & 0 & 1 & \cdots & 0 \\ \vdots & \vdots & \vdots & \vdots & \vdots & \ddots & \\ 0 & 0 & 0 & 0 & 0 & 0 & 1 \end{bmatrix} \tag{16}$$

Aided by Eqs. (14)-(16), the Jacobian matrix **A** can be found to be

$$\mathbf{A} = \begin{bmatrix} 0 & 1 & 0 & 0 & 0 & \cdots & 0 \\ -v^2\left(1-\frac{p_e}{2\rho}\right)+p_\rho+-\frac{e}{\rho}p_e & v\left(2-\frac{p_e}{\rho}\right) & \frac{p_e}{\rho} & p_{\rho 1} & p_{\rho 2} & \cdots & p_{\rho N_S-1} \\ v\left(-H+p_\rho+\frac{v^2}{2\rho}p_e-\frac{e}{\rho}p_e\right) & H-\frac{v^2}{\rho}p_e & v\left(1+\frac{p_e}{\rho}\right) & vp_{\rho 1} & vp_{\rho 2} & \cdots & vp_{\rho N_S-1} \\ -\frac{v}{\rho}\rho_1 & \frac{\rho_1}{\rho} & 0 & v & 0 & \cdots & 0 \\ -\frac{v}{\rho}\rho_2 & \frac{\rho_2}{\rho} & 0 & 0 & v & \cdots & 0 \\ \vdots & \vdots & \vdots & \vdots & \vdots & \ddots & \\ -\frac{v}{\rho}\rho_{N_S-1} & \frac{\rho_{N_S-1}}{\rho} & 0 & 0 & 0 & & v \end{bmatrix} \tag{17}$$

The eigenvalues of the matrix **A** and $\tilde{\mathbf{A}}$ Aare found to be

$$\lambda = \left(v \pm a, v, v \ldots v\right)^T \tag{18}$$

where v is the local velocity and a is the local speed of sound. Since the CESE method required that the CFL number to be less than or equal to 1.0. The CFL number is calculated by

$$\mathrm{CFL} = \max(\lambda)\frac{\Delta t}{\Delta x} = \left(|v| + a\right)\frac{\Delta t}{\Delta x} \tag{19}$$

B. Chemical Reactions

The reactions are governed by the law of mass action, which states that an elementary reaction can be written as

$$\sum_{i=1}^{N_S} \nu'_{ji}\frac{\rho_i}{M_i} \underset{K_{bj}}{\overset{K_{fj}}{\rightleftharpoons}} \sum_{i=1}^{N_S} \nu''_{ji}\frac{\rho_i}{M_i} \qquad j = 1, 2, \ldots, N_R \tag{20}$$

where ν_{ji}' and ν_{ji}'' are the stoichiometric coefficients of species i for the reactant and the product of reaction j, respectively. M_i is the molecular weight of species i. K_{fj} and K_{bj} are the forward and the backwards reaction rates, respectively. The reaction rate is formulated in the Arrhenius form:

$$K_{fj} = A_{fj}T^{n_{fj}}e^{\left(\frac{E_{fj}}{R_c T}\right)} \tag{21}$$

where A_{fj}, n_{fj} and E_{fj} are the Arrhenius coefficient, the temperature exponent, and the activation energy, respectively. These constants are supplied by the chemical mechanism employed. R_c is the universal gas constant, denoted with a subscript c because it uses calories, not joules, for energy in the units. The reverse reaction normally does not have an explicit form and has to be calculated through chemical equilibrium.

$$K_{b_j} = \frac{K_{f_j}}{K_{c_j}} \tag{22}$$

where K_{cj} is the equilibrium constant and is calculated by

$$K_{C_j} = \left(\frac{p_o}{RT}\right)^{\sum_{i=1}^{N_S} \nu_{ji}} e^{\left(\frac{-\Delta G_j}{RT}\right)} \tag{23}$$

where p_o is the reference pressure and ΔG_i is the difference in Gibbs energy between the products and the reactants of reaction j. ν_{ji} is defined as

$$\nu_{ji} = \nu''_{ji} - \nu'_{ji} \tag{24}$$

In our code, the calculations of the forward and backward reaction rates as well as the thermodynamic properties are handled by Cantera[15], an open source chemical kinetics package. The source terms $\dot{\omega}_i$ is calculated by

$$\dot{\omega}_i = M_i \sum_{j=1}^{N_R} \nu_{ni} \left[K_{f_j} \prod_{l=1}^{N_S} \left(\frac{\rho_l}{M_l}\right)^{\nu'_l} - K_{b_j} \prod_{l=1}^{N_S} \left(\frac{\rho_l}{M_l}\right)^{\nu''_l} \right] \tag{25}$$

In order to find the source term at the next time step, the time interval for the CFD calculation is subdivided into many sub-time steps for higher resolution of the chemical reactions. For each sub-time step, the species concentrations are approximated by

$$\mathbf{U}^{k+1} = \mathbf{U}^k + \Delta\mathbf{U}^k \tag{26}$$

where $\mathbf{U}^k = \left(\rho_1^k, \rho_2^k, ..., \rho_{N_S}^k\right)^T$ and $\mathbf{U}^{k+1} = \left(\rho_1^{k+1}, \rho_2^{k+1}, ..., \rho_{N_S}^{k+1}\right)^T$ and $\Delta\mathbf{U}$ is defined as

$$\Delta\mathbf{U}^k = \int_{t_1}^{t_2} \mathbf{S}(\mathbf{U}) dt = \frac{\Delta t_c}{2}\left(\mathbf{S}^k + \mathbf{S}^{k+1}\right) \tag{27}$$

where $\mathbf{S}^{k+1}$ is source term evaluated at k+1 sub-time step. It is approximated based on the first-order Taylor series expansion:

$$\mathbf{S}^{k+1} = \mathbf{S}^k + \left(\frac{\partial \mathbf{S}}{\partial \mathbf{U}}\right)\Delta\mathbf{U}^k \tag{28}$$

The combination of the above three equations forms an integration scheme based on the trapezoidal rule. They can be succinctly expressed as

$$\left[\frac{I}{\Delta t_c} - \frac{1}{2}\left(\frac{\partial \mathbf{S}}{\partial \mathbf{U}}\right)\right]\Delta\mathbf{U}^k = \mathbf{S}^k \tag{29}$$

To solve this equation, we use Newton's method. We remark that the term in the bracket represents a square matrix of rank N_S-1, in which the term $\frac{\partial \mathbf{S}}{\partial \mathbf{U}}$ is the chemical Jacobian and is calculated by

$$\left(\frac{\partial S_i}{\partial u_k}\right) = M_i \sum_{j=1}^{N_R} \nu_{ri} \left[\frac{\nu'_{jl} K_{f_j}}{\rho_k} \prod_{l=1}^{N_S} \left(\frac{\rho_l}{M_l}\right)^{\nu'_{jl}} - \frac{\nu''_{jl} K_{b_j}}{\rho_k} \prod_{l=1}^{N_S} \left(\frac{\rho_l}{M_l}\right)^{\nu''_{jl}} \right] \tag{30}$$

This equation can be derived by taking the derivative of equation (25) with reference to ρ_k.

III. CESE Method with Sub-time Steps

Originally developed by Chang[16], the CESE method is an explicit method for time accurate solution of nonlinear hyperbolic systems of partial differential equations (PDE). The method has also been extended for solution of systems of PDE with stiff source terms, e.g., the Euler equations for chemically reacting flows[17]. One of the major advantages of the CESE scheme is its ability to capture shock waves without using a Riemann solver[18]. This makes the CESE scheme numerically inexpensive and particularly suitable for reacting flows due to complex eigensystem of the modeling equations.

A. CESE Scheme for the Chemically Reacting Euler Equations

In this section, we illustrate the one-dimensional CESE method for solving the model equations Eq. (1). By using Gauss' divergence theorem, we recast Eq. (1) into a space-time integral form:

$$\int_{\partial S(V)} \mathbf{h}_m \cdot d\mathbf{s} = \int_{S(V)} s_m d\Omega \tag{31}$$

where V is a space-time domain and $S(V)$ is the surface of V. $\mathbf{h}_m = (u_m, f_m)^{\mathrm{T}}$ is the space-time flux vector with u_m and f_m as the m^{th} component of **U** and **F,** respectively. Components of **U** and **F** are shown in Eqs. (2) and (3). Figure 3 is schematic of the space-time integration by Eq. (31).

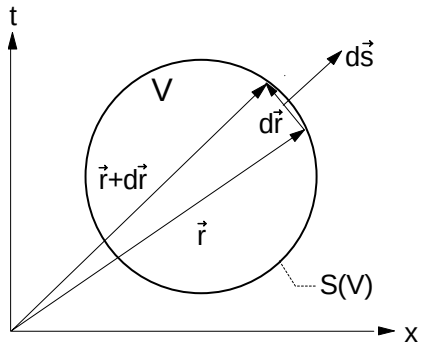

Figure 3: A schematic of the space-time integral.

Here $S(V)$ is the boundary of an arbitrary space-time region V, $d\vec{s}=d\sigma\vec{n}$ with $d\sigma$ being the area and $\vec{n}$ the normal vector. The CESE method treats space and time as one unity. Therefore, there is no restriction on the geometry of the conservation element. The flow variables are considered to be continuous inside a solution element (SE) and are represented by a first-order Taylor series expansion. For all $(x,t) \in SE(j,n)$, let $\mathbf{U}(x,t)$ be approximated by $\mathbf{U}^*(x,t)$.

$$u^*(x,t;j,n) = u_j^n + (u_x)_j^n (x - x_j) + (u_t)_j^n (t - t^n) \tag{32}$$

for all $(x,t) \in \mathrm{SE}(j,n)$. It is necessary to express f_m as a function of u_k to do this we let $(f_m)_j^n$ and $(f_{m,k})_j^n$ represent the value of f_m and $\partial f_m / \partial u_k$ for $m, k = 1,\ldots,N_s+2$ respectively also let $(u_m)_j^n$ be equal to u_m. Since

$$\frac{\partial f_m}{\partial x} = \sum_{k=1}^{N_s+2} \frac{\partial f_m}{\partial u_k}\frac{\partial u_k}{\partial x} \text{ and } \frac{\partial f_m}{\partial t} = \sum_{k=1}^{N_s+2} \frac{\partial f_m}{\partial u_k}\frac{\partial u_k}{\partial t} \tag{33}$$

the terms f_{mx} and f_{mt} can be rewritten as

$$(f_{mx})_j^n = \sum_{k=1}^{N_s+2} (f_{m,k})_j^n (u_{kx})_j^n \tag{34}$$

and

$$(f_{mt})_j^n = \sum_{k=1}^{N_s+2} (f_{m,k})_j^n (u_{kt})_j^n \tag{35}$$

As a result f_{mx} and f_{mt} are the numerical counterparts of $\partial \mathrm{fm}/\partial \mathrm{fx}$ and $\partial \mathrm{fm}/\partial \mathrm{ft}$ respectively. This allows us to write

$$f_m^*(x,t;j,n) \approx (f_m)_j^n + (f_{mx})_j^n (x - x_j) + (f_{mt})_j^n (t - t^n) \tag{36}$$

Since f_m, f_{mx}, f_{mt} are functions of u_m, u_{mx} and u_{mt} only. For all $(x,t) \in \mathrm{SE}(j,n)$ $u_m = u_m^*(x,t;j,n)$, $f_m = f_m^*(x,t;j,n)$ and $\tau_m = \tau_m^*(x,t;j,n)$ must satisfy Eq. (1) such that

$$\frac{\partial u_m^*(x,t;j,n)}{\partial t} + \frac{\partial f_m^*(x,t;j,n)}{\partial x} = \tau_m^*(x,t;j,n) \tag{37}$$

This requires two independent marching variables u_j^n and $(u_x)_j^n$ associated with each grid point. Since $\mathbf{h}_m = (u_m, f_m)^{\mathrm{T}}$ we define $\mathbf{h}^*_m(x,t;j,n) = (u^*_m, f^*_m)^{\mathrm{T}}$. Furthermore Gauss' theorem is applied to $\mathbf{h}^*$ resulting in

$$\int_{S(CE(j,n))} \mathbf{h}^* \cdot d\vec{s} = \int_{CE(j,n)} \tau(u)\, dV \tag{38}$$

The grid is made up of non-overlapping conservation elements, CE, which are rectangular in shape and an inverted T shaped SE. It should be noted that the CE fills the entire domain while the SE does not. The shape of the SE is chosen such that there is no source term present which allows the source term to be known at the current time step. If this were not the case then a there would be unknowns on the RHS of Eq. (38) which would require a Newton method to find the flow variables. The domain and the CE, SE are shown in Figure 4.

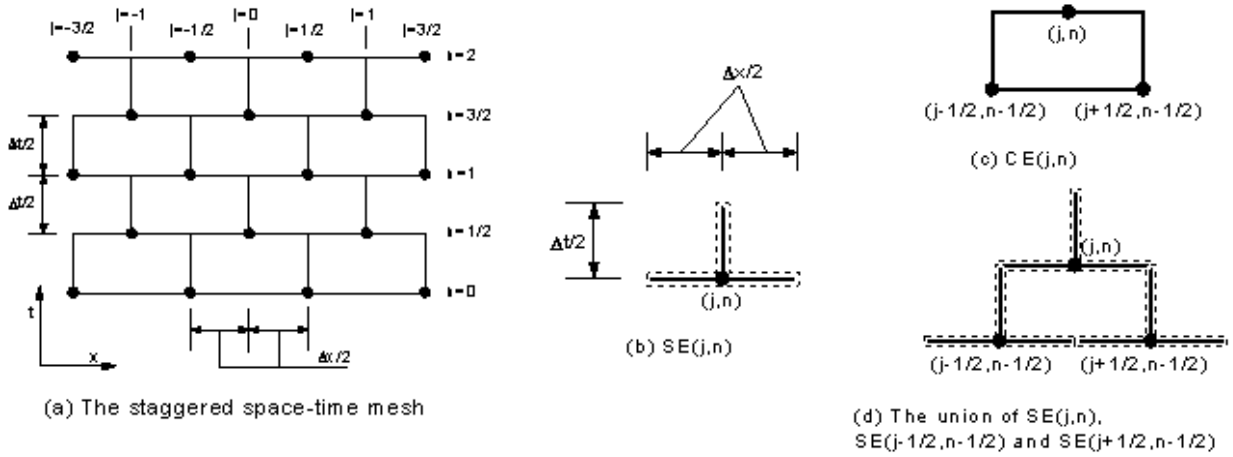

Figure 4: Space-time mesh of the CESE method.

Applying the flux conservation represented by Eq. (38) the time progression of u_m is equivalent to

$$\left(u_m\right)_j^n = \frac{1}{2}\left[\left(u_m\right)_{j-1/2}^{n-1/2} + \left(u_m\right)_{j+1/2}^{n-1/2} + \left(s_m\right)_{j-1/2}^{n-1/2} + \left(s_m\right)_{j+1/2}^{n-1/2} + \int_{n-\frac{1}{2}}^{n} \tau(u)_{j-1/2}\,dt + \int_{n-\frac{1}{2}}^{n} \tau(u)_{j+1/2}\,dt\right] \tag{39}$$

where

$$\left(s_m\right)_{j\pm1/2}^{n-1/2} = \frac{\Delta x}{4}\left(u_{mx}\right)_{j\pm1/2}^{n-1/2} + \frac{\Delta t}{\Delta x}\left(f_m\right)_{j\pm1/2}^{n-1/2} + \frac{\Delta t^2}{4\Delta x}\left(f_{mt}\right)_{j\pm1/2}^{n-1/2} \tag{40}$$

and $\int_{n-1/2}^{n} \tau\left(u\right)_j\,dt$ is evaluated by recalculating Eqs. (29) and (30) until the chemistry has progressed $\Delta t/2$ at each spatial location. In the example shown in Figure 5 there are four chemistry time steps for every physical time step, i.e. $\Delta t_c = 0.25\Delta t$.

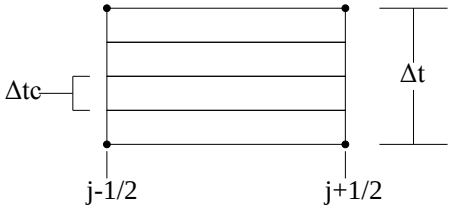

Figure 5: The sub-time steps for calculating chemical reactions.

There are several different methods used to re-weight u_{mx}. They differ by how they suppress overshoot around discontinuities. In a recent paper Chang and Wang proposed 4 different schemes w-1, w-2, w-3 and w-4[19]. Currently w-2 and w-4 methods have been implemented. The w-2 CFL insensitive scheme is shown below

$$\left(u_x\right)_j = \frac{\left|\left[q_+ - \left(u_m\right)_j\right]\frac{2}{\Delta x}\right|^{\alpha} P_- + \left|\left[\left(u_m\right)_j - q_-\right]\frac{2}{\Delta x}\right|^{\alpha} P_+}{\left|\left[q_+ - \left(u_m\right)_j\right]\frac{2}{\Delta x}\right|^{\alpha} + \left|\left[q_+ - \left(u_m\right)_j\right]\frac{2}{\Delta x}\right|^{\alpha}} \tag{41}$$

where α is either 1 or 2 and

$$q_{\pm} = \left(u_m\right)_{j\pm1/2} + \frac{\Delta t}{2}\left(\frac{du}{dt}\right)^{n-1/2}_{j\pm1/2} \tag{42}$$

and

$$P_{\pm} = \left(\mp\left(u_m\right)_j \pm q_{\pm}\right)\left(\frac{4}{\Delta x}\frac{1}{1+\nu_j}\right)\mp\left(\frac{du}{dx}\right)^{n-1/2}_{j\pm1/2} \tag{43}$$

For a full derivation and the other re-weighting schemes refer to Chang[19].

IV. Results and Discussion

With CFD simulations it is important to determine the required spatial and temporal distribution that will produce accurate yet prompt results. The present CFD solver has two dimensions: space, Δx, and time, Δt. On the other hand, the chemistry solvers have only one dimension time, Δtc. The first step in optimization is to determine the maximum Δx and Δt for the CFD solver. The time step found by solving Eq. (19) for Δt, since Δx is constant in the domain the eigenvalue chosen is the maximum in the entire domain. Generally the target CFL number should be very close to 1.0 but due to rapid increases in the speed of sound and local velocity associated with the onset of combustion it was found that the target CFL number should not be greater than about 0.8. To optimize Δx the temperature history at a location of 2 mm from the end wall was compared at various Δx. When Δx was greater than $2.0\text{x}10^{-3}$ meters the grid point nearest to the end wall was chosen. The initial conditions used in the study are shown in Table 1. It can be seen in Figure 6 that the reflected temperatures converge at about $2.0\text{x}10^{-4}$ meters for both Case 1 and Case 2. It should also be noted that at a higher pressure ratio the solution diverges more quickly. For example at a Δx of $8.0\text{x}10^{-3}$ the error for Case 1 is about 2.5 K or 0.5% where as the error in Case 2 is about 15 K or 1.6%. Although the percentage error is small a 15 K difference in temperature will cause a significant difference in the ignition time.

Table 1: Initial conditions used to optimize the spatial distribution of points.

	Case 1		Case 2	
	Driver	Driven	Driver	Driven
T (K)	300	300	300	300
P (atm)	1.0	0.1	10.0	0.1
Species	Air	Air	Air	Air

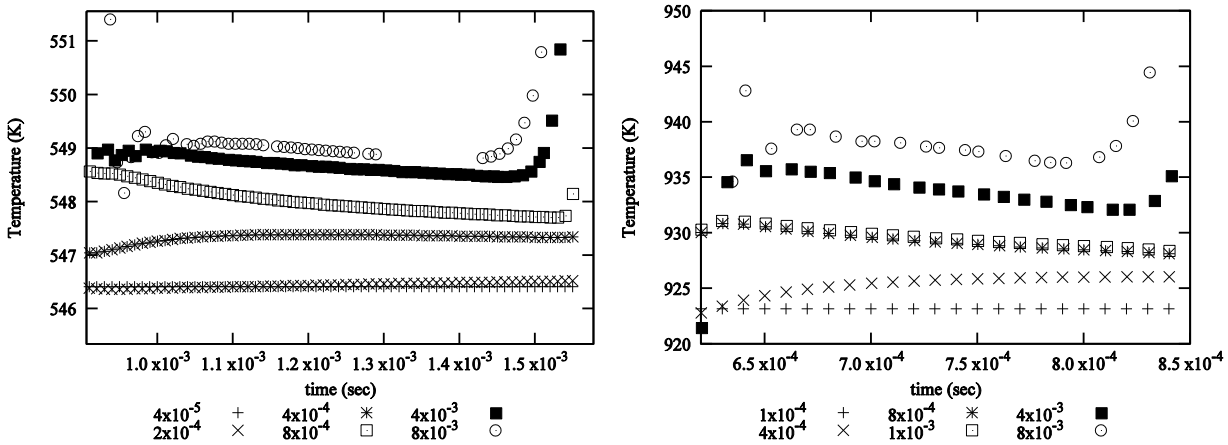

Figure 6. Temperature history near the end wall at various Δx (m) Case 1 (left) and Case 2 (right).

The effect of the CFL number is also important because a lower CFL number should also decrease the error. To test this, Δx was held constant at $8.0\text{x}10^{-3}$ and the CFL number was lowered by a factor of ten until the calculated temperature converged. The results in Figure 7 show that the results do improve as the CFL number is lowered but the CPU time also increases. It can also be seen that it is not more advantageous to run a simulation at a lower CFL

number and a higher Δx. The amount of CPU time required to run a simulation at a CFL number of 0.08 and a Δx of $8.0x10^{-3}$ is ~6 seconds, which is equivalent to the amount of CPU time required to run the simulation at a CFL of 0.8 and a Δx of $2.0x10^{-3}$ but the second setup has a smaller error.

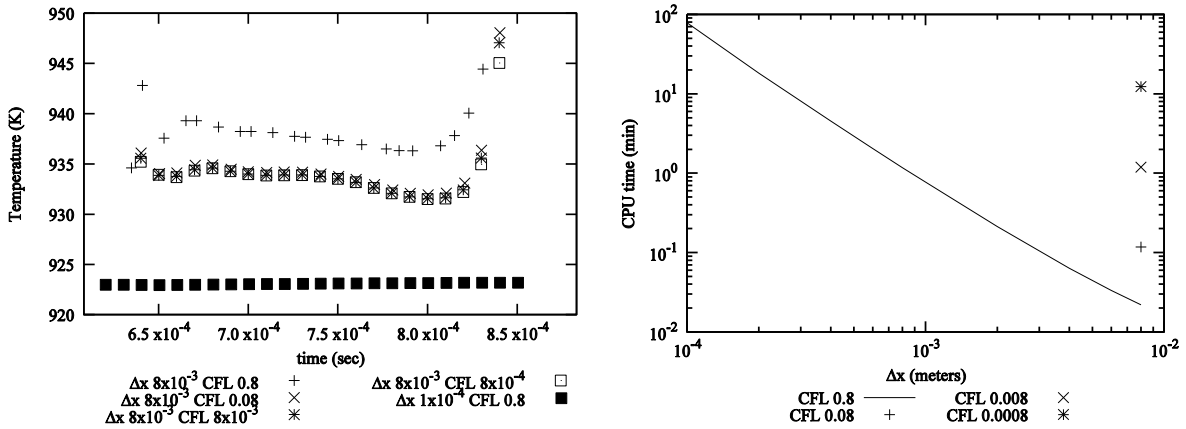

Figure 7. The effect of a lower CFL number on the reflected shock temperature (left) and the CPU time required to complete the calculation (right).

The next step in optimization is to determine the largest chemical time step and still remain numerically stable. This is accomplished by running a zero dimensional simulation and observing how well mass is conserved. The reason there is an error in mass conservation is that after the chemical calculations are performed some of the species may have a negative mass due to overshoot. Since mass cannot be negative those species masses are set to a small positive number, $1.0x10^{-14}$. Typically these negative masses are small so when the new mass is calculated the increase is very small but at the onset of combustion some of the species masses can have a large negative mass resulting in a larger error. The two cases shown in Figure 8 and Figure 9 were run at an equivalence ratio of 1, a pressure of 1 atm, as well as three different temperatures, 1100, 1500 and 2000 K. This set up was run twice once with a bath gas, Ar, percent of 85 and 95 percent for ZeroD case 1 and 2 respectfully. The percentage of the bath gas present has a larger impact on the maximum possible chemical time step than the initial temperature of the gas. The numerical stability translates well to the numerical accuracy. The percent error shown in Figure 9 was determined by the difference in time that it takes for the temperature to rise 200 K. The chemical mechanism chosen to model the C_2H_4 reactions was created by Wang and Laskin[12]. This mechanism was chosen because it is smaller than Wang's newer version which allows for more simulations to be done in a shorter time span.

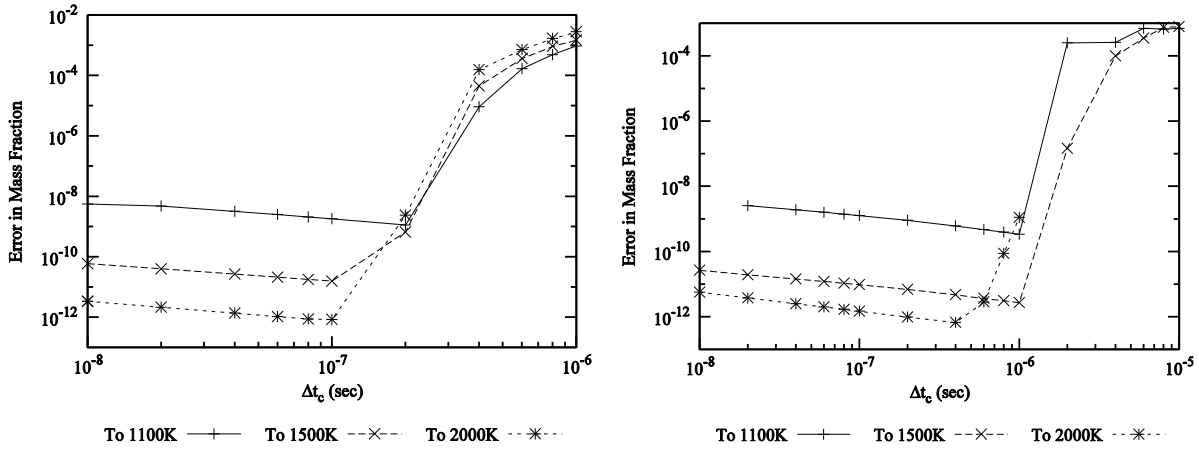

Figure 8. The effects of the chemical step on the conservation of mass, left ZeroD case 1 right case 2.

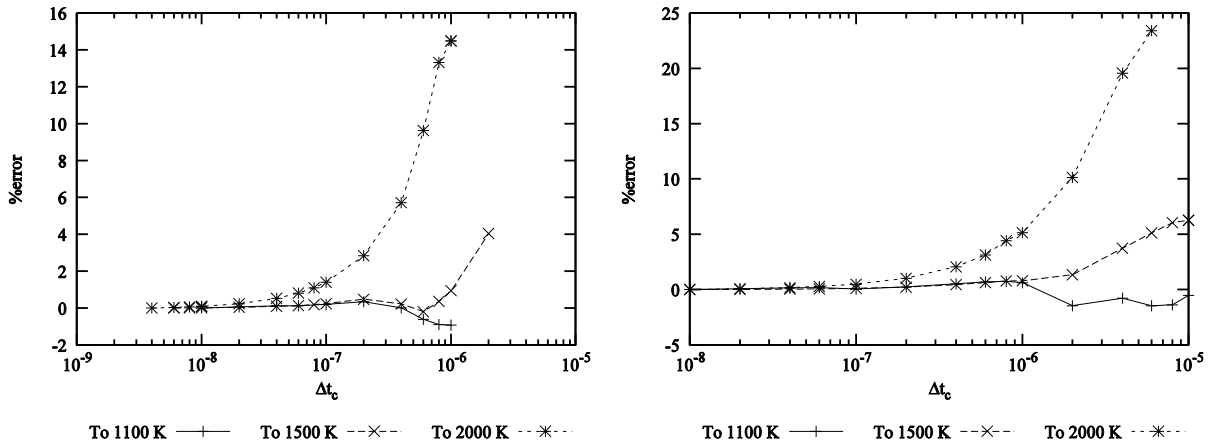

Figure 9. Percent different from smallest time step, left ZeroD case 1 right case 2.

To summarize the following paragraphs the optimum $\Delta x \cong 2.0x10^{-4}$ meters and the optimum $\Delta tc \cong 1.0x10^{-7}$ seconds. One particular shock tube set up was chosen to test how well the zero dimensional combustion calculations and the frozen shock tube simulations where at predicting an accurate Δx and Δtc. Figure 10 shows the same calculations using multiple Δx and Δtc as well as the induction times predicted by a zero dimensional simulation ran at constant pressure and constant volume. A best fit line is also included on this plot. The initial set up for the shock tube and the properties in different sections are shown in Table 2, all properties are calculated by the CFD simulation. Given the spread in the data shown in Figure 10 it is difficult to make a definitive statement but it can be seen that a $\Delta tc \geq 1.0x10^{-7}$ seconds is too large but that a Δx of $4.0x10^{-4}$ meters still predicts accurate results. These results are different from what was predicted by the frozen shock tube simulations and the zero dimensional calculations. It should be noted that due to wave interactions the combusted gas did not come to an equilibrium point. Because of this the induction time noted in Figure 10 is when the OH mole reaches 90% of its max value and not the steady state value. There was no notable difference when the mole fraction was used instead of the molar concentration. The induction time for the constant volume calculation was defined as the time it takes for the temperature to rise 200 K.

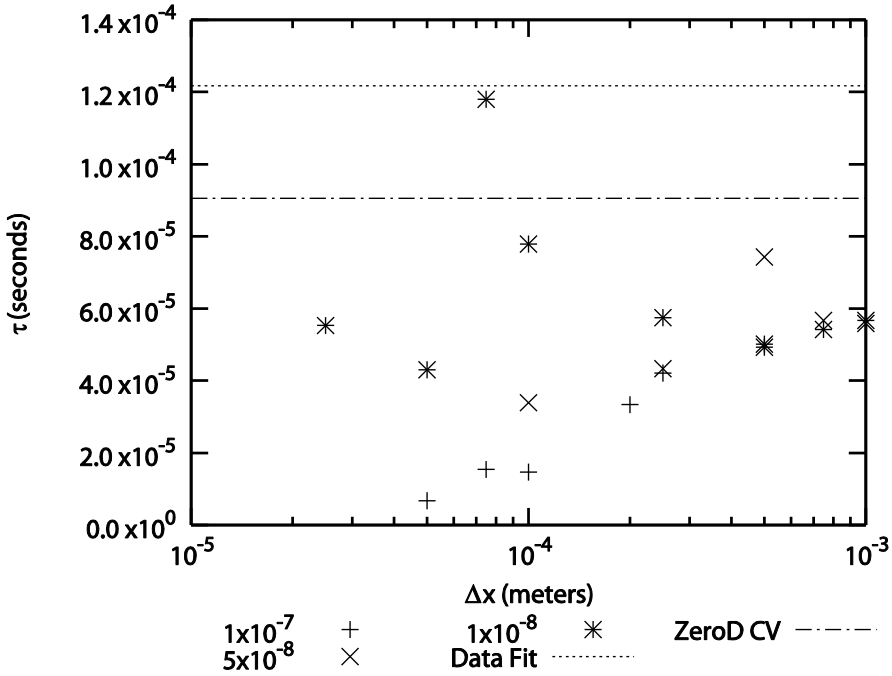

Figure 10. Induction times for a shock tube simulation with various Δx and Δt_c.

Table 2. Shock tube setup for testing required Δx and Δt_c.

	Driver	Driven	Shocked	Reflected
T (K)	300	300	850	1528
P (atm)	1.4	0.04	0.32	1.28
Species	He/C_3H_8 0.84/0.16	$C_2H_4/O_2/Ar$ 0.0125/0.0375/0.95	$C_2H_4/O_2/Ar$ 0.0125/0.0375/0.95	$C_2H_4/O_2/Ar$ 0.0125/0.0375/0.95

The equation for the induction delay time shown in Figure 10 is[12]

$$\tau(\mu s) = 10^{-57.97} T^{14.854} \exp\left(\frac{35900}{T}\right)[C_2H_4]^{0.230}[0_2]^{-0.839}[Ar]^{0.247} \tag{44}$$

In order to ascertain the accuracy of the shock tube tool several Methane simulations where ran. Methane was chosen because it has been well studied under several different conditions and an accurate mechanism exists. The mechanism chosen to model Methane was the Gri Mech 3.0[13]. Preliminary testing, Figure 11, has shown good agreement between numerical simulations and shock tube experiments for methane oxygen reactions. The paper by Spadaccini[3] collected shock tube results from over 500 different experiments and found that the equation originally developed by Lifshitz et.al and improved upon by Krishnan and Ravikumar provided a reasonable ignition time from a temperature of 1250 to 2500 K. Although they found that the equation tends to under predict the induction time when the temperature becomes lower. The data fit on Figure 11 was calculated from[3]

$$\tau = 2.21\times10^{-14} \exp\left(\frac{22659}{T}\right)[O_2]^{-1.05}[CH_4]^{0.33} \tag{45}$$

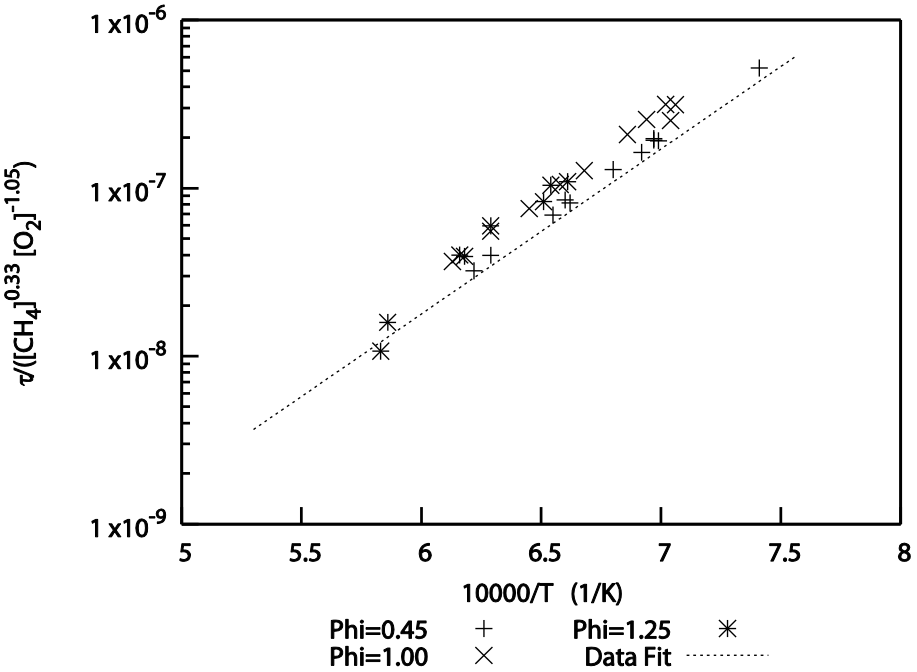

Figure 11. Induction times for CH_4-O_2 reactions at various initial temperatures and pressures.

V. Conclusion

The present paper reports the development of a new numerical shock-tube tool to facilitate the development of the scramjet engine. The code was developed based on the use of the CESE method for solving the flow equations in conjunction with an implicit trapezoidal rule and sub-time steps for integrating the stiff ODE for chemistry models. Numerical results of methane/air and ethane/air combustion inside of a shock tube have been carried out and reported. Flow physics in shock tube experiments were recreated and the calculated ignition delay times were compared with experimental data through a best-fit line. These preliminary results show the usefulness of our program. This numerical tool can be used to (i) test a wide range of fuel/air conditions, (ii) to serve as a test bed to assess the accuracy of the reduced chemistry models, and (iii) to facilitate the use of the shock tube experiments to study chemical reactions in heavy hydrocarbon fuels for the scramjet engines.

Acknowledgments

The first and second authors would like to thank the Dayton Area Graduate Studies Institute for providing the funding for this study.

References

[1]Kahandawala, M.S.P, DeWitt, M.J., Corporan, E., Sidhu, S.S., "Ignition and Emission Characteristics of Surrogate and Practical Jet Fuels", *Energy Fuels*, 22 (2008), 6 3673-3579.

[2]Li, H., Owens, Z.C., Davidson, D.F., Hanson, R.K., "A Simple Reactive Gasdynamic Model for the Computation of Gas Temperature and Species Concentrations behind Reflected Shock Waves", *Int. J. of Chemical Kinetics*, 40 (2008):189-198.

[3]Spadaccini, L.J., and Colket III, M. B., "Ignition Delay Characteristics of Methane Fuels." *Progress in Energy Combustion Science* 20 (1994): 431-460.

[4]McClinton, Charles R., "*X-43-Scramjet Power Breaks the Hypersonic Barrier Dryden Lectureship in Research for 2006*," 44th AIAA Aerospace Sciences Meeting and Exhibit, 2006.

[5]Hank, Joseph M., Murphy, James S., Mutzman, Richard C., "The X-51A Scramjet Engine Flight Demonstration Program," *15th AIAA International Space Planes and Hypersonic Systems and Technologies Conference*, 2008.

[6]Edwards, E., Anderson, S.D. "Results of High Temperature JP-7 Cracking Assessment", *AIAA 31st Aerospace Sciences Meeting*, AIAA, Washington, D.C., 1993, pp. 1,6

[7]Puri, P., Ma, F., Choi, J., Yang, Vi., "Ignition Characteristics of cracked JP-7 fuel", *Combustion and Flame*, Vol. 142, June 2005 pp. 454-457.

[8]Colket III, M.B., Spadaccini L.J., "Scramjet Fuels Autoignition Study", *Journal of Propulsion and Power*, Vol. 17, No. 2, March 2001.

[9]Kahadawala, Moshan S.P., Shehan A. P. Corera, Skip Williams, Campbell D. Carter, and Sukh S. Sidhu. "Investigation of Kinetics of Iso-Octane Ignition under Scramjet Conditions." *International Journal of Chemical Kinetics* 38, no. 3 (2006): 194-201.

[10]Gaydon, A.G., Hurle, I.R., *The Shock Tube in High-Temperature Chemical Physics*, 1st ed., Reinhold Publishing Corporation, New York, 1963, pp. 64, 98.

[11]Amadio, A.R., Crofton, M.W., Petersen, E.T., "Test-time Extension Behind Reflected Shock Waves Using CO_2-He and C_3H_8-He Driver Mixtures", *Shock Waves*, Vol. 16, 2006, pp. 157-165.

[12]Wang, Hai, Laskin, Alexander, A Comprehensive Kinetic Model of Ethylene and Acetylene Oxidation at High Temperatures. Mechanical Engineering Dept. University of Delaware, URL: http://ignis.usc.edu/Mechanisms/C2-C4/c2.html, (accessed October 2008).

[13]Smith, Gregory P., et.al., GRI-MECH 3.0 UC Berkely, URL: http://www.me.berkeley.edu/gri-mech/version20/text30.html (accessed November 2008)

[14]Bilyeu, D.L., "Numerical Simulation of Chemical Reactions Inside a Shock-Tube by the Space-Time Conservation Element and Solution Element Method", Master's Thesis, Mechanical Engineering Dept., The Ohio State University, OH, 2008.

[15]Cantera, Software Package, Version 1.7.1, Goodwin, David G, URL: http://sourceforge.net/projects/cantera (last accessed November 03, 2008).

[16]Chang, S.-C. "The Method of Space-Time Conservation Element and Solution Element - A New Approach for Solving the Navier-Stokes and Euler Equations." *Journal of Computational Physics*, 1995: 295-324.

[17]Yu, S.T., S.C. Chang, and. Jorgenson, P.C.E., "Direct Calculation of Detonation with Multi-Step Finite-Rate Chemistry by the Space-Time Conservation Element and Solution Element Method," *AIAA 30th. Fluid Dynamics Conference and Exhibit*. AIAA, 1999.

[18]Chang, S-C, "On Space-Time Inversion Invariance and its Relation to Non-Dissipatedness of a CESE Core Scheme," *42th AIAA/ASME/SAE/ASEE Joint Propulsion Conference and Exhibit*, 2006.

[19]Chang, S-C, Wang X.Y., "Multi-Dimensional Courant Number Insensitive CE/SE Euler Solvers for Applications Involving Highly Nonunirorm Meshes," *39th AIAA/ASME/SAE/ASEE Joint Propulsion Conference and Exhibit*, 2003.